DEVELOPMENTAL NEUROSCIENCE

Neuroinflammatory signals drive spinal curve formation in zebrafish models of idiopathic scoliosis

J. L. M. Van Gennip[1,2]*, C. W. Boswell[1,2]*, B. Ciruna[1,2†]

The etiopathogenesis of idiopathic scoliosis (IS), a highly prevalent spinal deformity that occurs in the absence of obvious congenital or physiological abnormalities, is poorly understood. Although recent zebrafish genetic studies have linked cilia motility and cerebrospinal fluid (CSF) flow defects with scoliosis progression, underlying mechanisms were not identified. Here, we use next-generation sequencing and conditional genetic methodologies to define the spatial and biological origins of spinal curve formation in *ptk7* mutant zebrafish, a faithful IS model. We demonstrate that focal activation of proinflammatory signals within the spinal cord is associated with, and sufficient for, induction of spinal curvatures. Furthermore, administration of acetylsalicylic acid (aspirin) or *N*-acetylcysteine (NAC) to juvenile *ptk7* mutants significantly reduces the incidence and/or severity of scoliosis phenotypes. Together, our results implicate neuroinflammation, downstream of CSF defects, in spinal curve formation and provide intriguing evidence that simple immunomodulating therapies might prove effective in managing idiopathic-like spinal deformities.

INTRODUCTION

Idiopathic scoliosis (IS) is characterized by rotational deformities of the spine that arise in the absence of congenital vertebral malformations or other obvious neuromuscular or physiological defects. IS afflicts ~4% of the population, although curve severity, rotational complexity, and age of onset differ among individuals (*1*). Genetic studies have linked multiple loci with broad physiological implications to IS progression, including rare variants in genes associated with centriole (*POC5*) (*2*) and musculoskeletal collagen function (*3*), as well as noncoding mutations associated with *GPR126*, *PAX1*, *LBX1*, and *BNC2*, genes that play varied roles in bone, cartilage, muscle, and nervous system development (*4*–*7*). Nevertheless, biological mechanisms underlying IS are not understood and, as a result, treatment options remain limited to antiquated measures such as restrictive brace wear and invasive surgical correction (*1*).

Recently, zebrafish have emerged as a powerful model for probing the genetic and biological mechanisms underlying IS-like spinal deformities (*8*). Notably, zebrafish *protein tyrosine kinase 7* (*ptk7*) mutants, deficient in a key regulator of Wnt signal transduction (*9*), develop late-onset spinal curvatures that faithfully recapitulate defining aspects of human IS (*10*). Wnt signals control the biogenesis and polarized architecture of motile cilia (*11*), and analysis of *ptk7* mutants, as well as additional zebrafish models of IS, revealed a surprising link between motile cilia–driven cerebrospinal fluid (CSF) flow defects and scoliosis (*12*). Reintroduction of Ptk7 specifically within motile ciliated cell lineages of *ptk7* mutant animals (using a *foxj1a::ptk7* transgene) rescued ependymal cell cilia function, restored CSF flow through adult brain ventricles, and fully suppressed spinal curve formation. As human congenital defects that disrupt CSF flow (Chiari malformation, syringomyelia, and spina bifida) (*13*–*15*) also associate with high incidences of developmental scoliosis, zebrafish IS studies predict an evolutionarily conserved function for CSF flow and/or homeostasis in normal spine development (*12*). However, pathobiological mechanisms underlying spinal curve formation remain unknown.

Using conditional genetic methodologies, we now demonstrate that normal spine morphogenesis requires Ptk7 function specifically within motile ciliated cell lineages of the brain, consistent with a role for CSF flow and/or homeostasis defects in IS pathogenesis. We further demonstrate that focal activation of proinflammatory signals within the spinal cord is associated with, and sufficient for, induction of idiopathic-like spinal curvatures. Together, our results implicate neuroinflammation, downstream of CSF defects, in spinal curve formation and provide intriguing evidence that simple immunomodulating therapies might prove effective in managing both the incidence and severity of IS-like spinal deformities.

RESULTS

Defining tissue-specific requirements for Ptk7 in normal spine morphogenesis

The suppression of scoliosis in *ptk7* + Tg(*foxj1a::ptk7*) zebrafish indicated an essential role for Ptk7 within *foxj1a*$^+$ motile ciliated cell lineages, which include the laterality organ, pronephric duct, and midline cells of the central nervous system (CNS), as previously scored by Tg(*foxj1a::eGFP*) reporter activity (*12*). However, additional *foxj1a*$^+$ cell populations (i.e., in vertebrae or supporting tissue) may have been overlooked in Tg(*foxj1a::eGFP*) transgenic animals because of weak or transient enhanced green fluorescent protein (eGFP) reporter expression. To comprehensively determine where Ptk7 may function in spine development, we traced the fates of all *foxj1a*-expressing cells. Transgenic fish expressing Cre recombinase under the *foxj1a* promoter (*foxj1a::iCre*) were generated and crossed to a ubiquitous *ubi:loxP-eGFP-loxP-mCherry* (*ubi:Switch*) reporter line (*16*) such that all *foxj1a*$^+$ cells are permanently labeled by mCherry expression. In larval- and juvenile-staged animals, mCherry was largely confined to the CNS and we failed to detect mCherry$^+$ cells within the bone, muscle, or cartilage around or within the spinal column (fig. S1). However, novel *foxj1a*$^+$ expression domains were observed within the spinal cord, lateral line, and motor neuron cell populations (fig. S1, B, C, and E″, and movie S1). Therefore, neurosensory or neuromuscular origins of scoliosis in *ptk7* models cannot be discounted.

[1]Program in Developmental & Stem Cell Biology, The Hospital for Sick Children, 686 Bay Street, Toronto, Ontario M5G 0A4, Canada. [2]Department of Molecular Genetics, University of Toronto, Toronto, Ontario M5S 1A8, Canada.
*These authors contributed equally to this work.
†Corresponding author. Email: ciruna@sickkids.ca

To further define the spatial requirements for Ptk7 in spine development, we developed a conditional genetic approach in which scoliosis in *ptk7* mutants is suppressed by a Cre-excisable *loxP-foxj1a::ptk7-loxP* (floxed-*foxj1a::ptk7*) transgene (fig. S2A). Early and ubiquitous Cre expression from a heat shock–inducible *hsp:Cre* transgene (*17*) can restore scoliosis in these mutant animals, indicating that the Tg(floxed-*foxj1a::ptk7*) cassette can be efficiently recombined in vivo (fig. S2, B and C). To restrict the temporal and spatial domains of Cre expression, we used a modified soldering iron strategy (*18*) and performed localized heat shocks on *ptk7* + Tg(floxed-*foxj1a::ptk7*) + Tg(*hsp:Cre*) + Tg(*ubi:Switch*) mutant embryos at 2.5 days post-fertilization (dpf), imaged for Cre recombination activity at 5 dpf, and grew animals with successful recombination to adulthood (Fig. 1, A to D, and fig. S2D). Trunk- and tail-specific recombination of Tg(floxed-*foxj1a::ptk7*), as reported by *Tg*(*ubi:Switch*) mCherry expression, failed to restore scoliosis phenotypes in all trials (Fig. 1, B and F; $n = 38$ of 38). In contrast, head-specific recombination of Tg(floxed-*foxj1a::ptk7*) restored IS phenotypes in *ptk7* mutants (Fig. 1, C and G; $n = 14$ of 49). Notably, *ptk7*/+ sibling controls that were locally heat shocked did not develop spinal curvatures (Fig. 1H; $n = 82$ of 82), indicating that scoliosis observed in experimental cohorts was specific to Tg(floxed-*foxj1a::ptk7*) recombination. Together, with lineage tracing experiments, our results indicate that Ptk7 is not required in the trunk peripheral nervous system, spinal cord, vertebrae, cartilage, or muscle for normal spine development. Rather, loss of Ptk7 specifically within *foxj1a*$^+$ lineages of the brain is sufficient to induce scoliosis.

As the brain and spine are spatially and functionally distinct, the pathogenesis of scoliosis in *ptk7* mutants likely involves secondary signals. Notably, *foxj1a*$^+$ lineage tracing broadly labels ependymal and choroid plexus cells within the brain, which function in the production and movement of CSF (fig. S1E′) (*19*), and CSF flow defects have been demonstrated within adult *ptk7* brain ventricles (*12*). To investigate whether CSF flow dynamics are abnormal in *ptk7* mutants at developmental stages relevant to scoliosis phenotypes, we performed live imaging of soluble dye injected into the brain ventricles of juvenile-staged zebrafish. Notably, severe defects in the movement of CSF into the spinal cord of *ptk7* mutants were observed before scoliosis onset (Fig. 1, I and J; $n = 12$ of 12), consistent with abnormalities of CSF flow and/or homeostasis contributing to the pathogenesis of IS.

Abnormal immune responses, downstream of CSF defects, associate with scoliosis

To identify molecular mechanisms underlying spine curvature, downstream of brain and/or CSF defects, we performed next-generation RNA sequencing (RNA-seq) on *ptk7* mutant versus *ptk7*/+ sibling fish at a stage correlating with severe IS progression (~1 cm in length; fig. S3B). Heads were dissected at the level of the gill to remove upstream

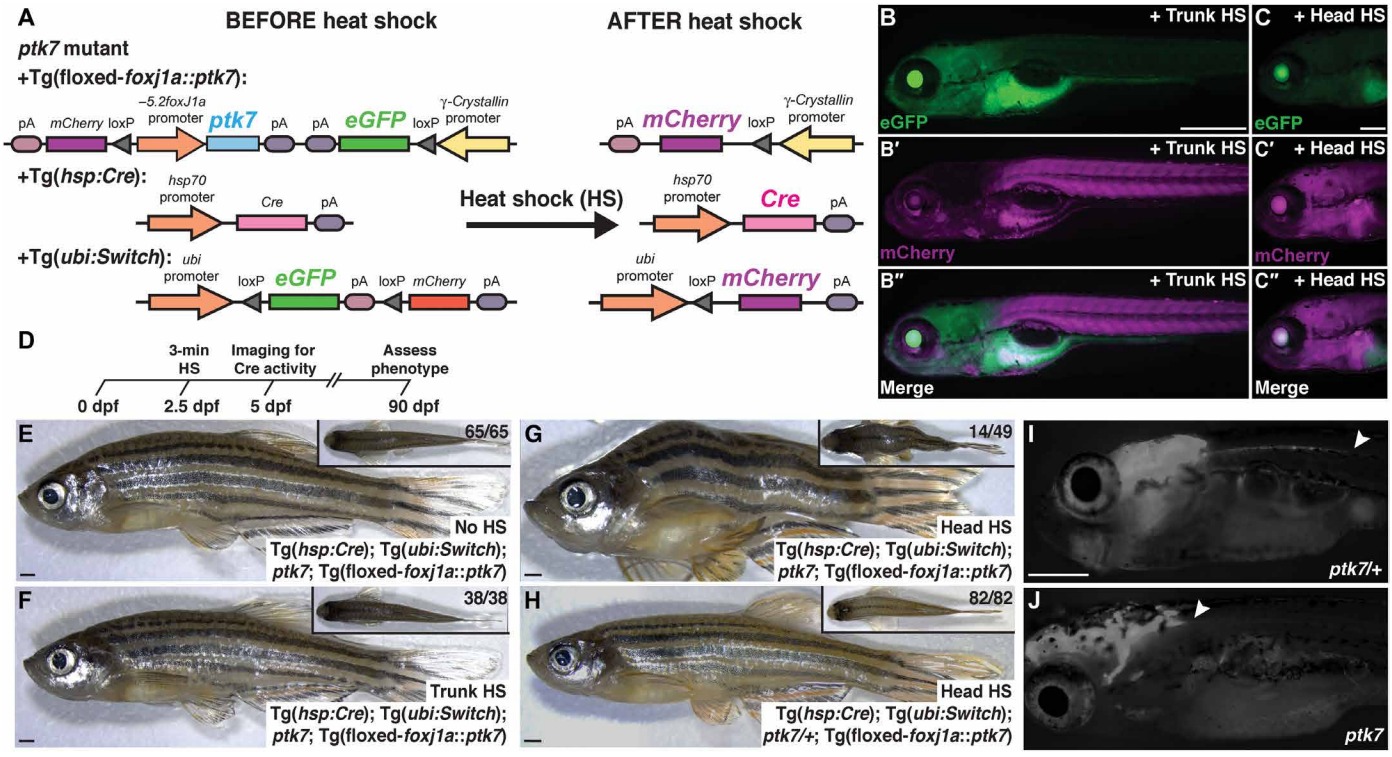

Fig. 1. Loss of Ptk7 in the head is sufficient to cause scoliosis. (**A**) Schematic of transgene-based conditional *ptk7* loss-of-function strategy. (**B** and **C**) Representative 5-dpf experimental larvae following trunk-specific (B and B″) and head-specific (C and C″) heat shock at 2.5 dpf. GFP to mCherry Tg(*ubi:Switch*) conversion reports localized Cre activity and the site of Tg(floxed-*foxj1a::ptk7*) recombination. (**D**) Experimental timeline of heat shock treatment. (**E** to **G**) Lateral views of adult *ptk7* mutant experimental fish following no heat shock (E), localized trunk heat shock (F), or head heat shock (G). (**H**) Lateral view of control *ptk7*/+ adult fish following head heat shock. (E to H) Photo Credit: C. W. Boswell, The Hospital for Sick Children. (**I** and **J**) Violet highlighter ink injected into the ventricle of 14-dpf juvenile animals reports movement of CSF down the spinal canal of *ptk7*/+ fish [white arrowheads; $n = 11$ of 12 (G)], which is absent in *ptk7* mutants [$n = 12$ of 12 (H)]. Photo Credit: J. L. M. Van Gennip, The Hospital for Sick Children. Scale bars, 500 μm (B, I, and J), 200 μm (C), and 1 mm (E to H).

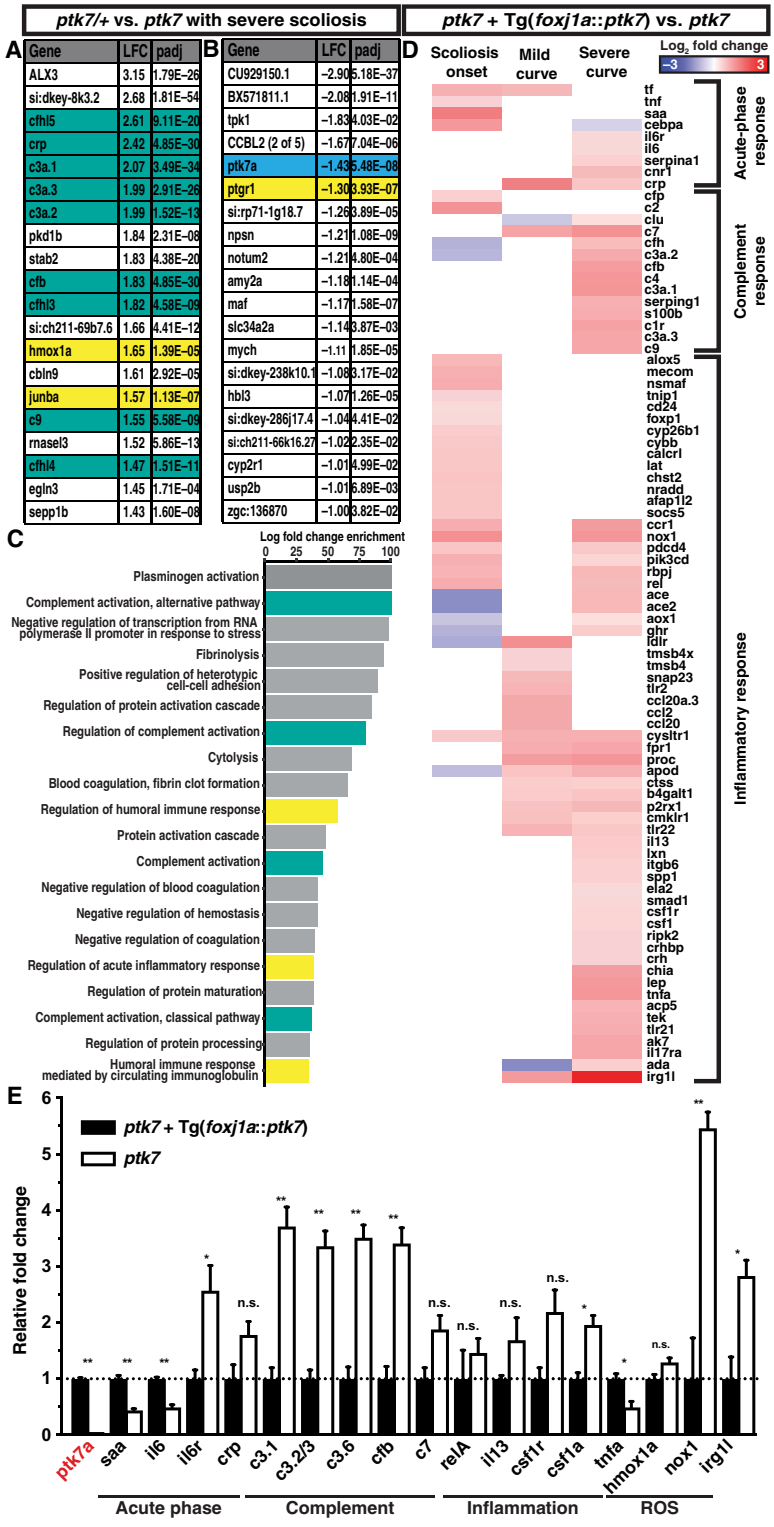

Fig. 2. Spinal curve progression is associated with immune and neuroinflammatory responses. (**A** and **B**) Top 20 significantly ($P < 0.05$) up-regulated (A) and down-regulated (B) genes [sorted by $\log_2$ fold change (LFC)] identified in *ptk7* mutant fish with severe spinal curvatures versus *ptk7*/+ control siblings. padj, Benjamini-Hochberg adjusted *P* value. (**C**) Gene Ontology (GO) term enrichment analysis of biological processes on all significantly up-regulated genes. Teal, complement response genes; yellow, other immune responses; blue, *ptk7*. (**D**) Heatmap depicting expression of immune and inflammatory response genes significantly ($P < 0.05$) up-regulated in *ptk7* mutants at curve onset or during mild and severe curve progression versus *ptk7* + Tg(*foxj1a::ptk7*) control siblings. (**E**) Quantitative reverse transcription polymerase chain reaction (qRT-PCR) verifying differential expression of selected genes in *ptk7* mutants with severe curves versus *ptk7* + Tg(*foxj1a::ptk7*) siblings. $^{*}P < 0.05$, $^{**}P < 0.01$. n.s., not significant.

signals associated with abnormal Ptk7 function in the brain, and because downstream cellular and biological origins of scoliosis remained unknown, RNA-seq was performed on bulk RNA samples collected from the entire trunk and tail. As expected, differential gene expression analysis revealed that *ptk7* mutant transcripts, which are subject to nonsense-mediated decay (*9*), are significantly reduced in scoliotic animals (Fig. 2B). Genes associated with bone, muscle, or connective tissue development were not significantly dysregulated in scoliotic fish (fig. S3, D to F). Rather, most of the transcripts significantly up-regulated in *ptk7* mutants encoded proteins involved in complement activation and innate immune response (Fig. 2, A to C; fig. S3C; and data file S1).

Because Ptk7 and Wnt signals control diverse biological activities across numerous tissues, abnormal immune responses observed in *ptk7* mutant fish might be unrelated to scoliosis phenotypes. To identify gene expression profiles directly associated with spinal curve progression, we repeated RNA-seq experiments comparing *ptk7* and *ptk7* + Tg(*foxj1a::ptk7*) mutant animals, which are genetically and phenotypically equivalent beyond *ptk7* transgene expression and spine development (fig. S4A) (*12*). RNA was collected from trunk and tail tissues at time points correlating with scoliosis onset (~0.7 cm in length; fig. S4B), as well as mild and severe curve progression (~0.8 cm in length; fig. S4, C and D). Notably, differential gene expression and qRT-PCR analyses confirmed a significant and dynamic scoliosis-associated immune response in *ptk7* mutants, including activation of acute-phase inflammation markers at the onset of spinal curvature, complement system activation at severe curve progression, and the up-regulation of NOD (nucleotide-binding oligomerization domain)–like receptors and other immune response genes across developmental time points (Fig. 2, D and E; fig. S4, E to G; and data file S1).

To determine how inflammation and immune responses correlate with spinal curvature, we directly monitored macrophage activity in juvenile *ptk7* mutant versus *ptk7*/+ sibling fish using the *mpeg1:eGFP* reporter transgene (*20*). Notably, eGFP$^+$ macrophages accumulated locally at the site of spinal curve formation in *ptk7* mutants (Fig. 3, A and B), consistent with an early role for inflammation in the pathogenesis of IS. Transverse sections through the trunks of these animals revealed increased accumulation of eGFP$^+$ macrophages specifically

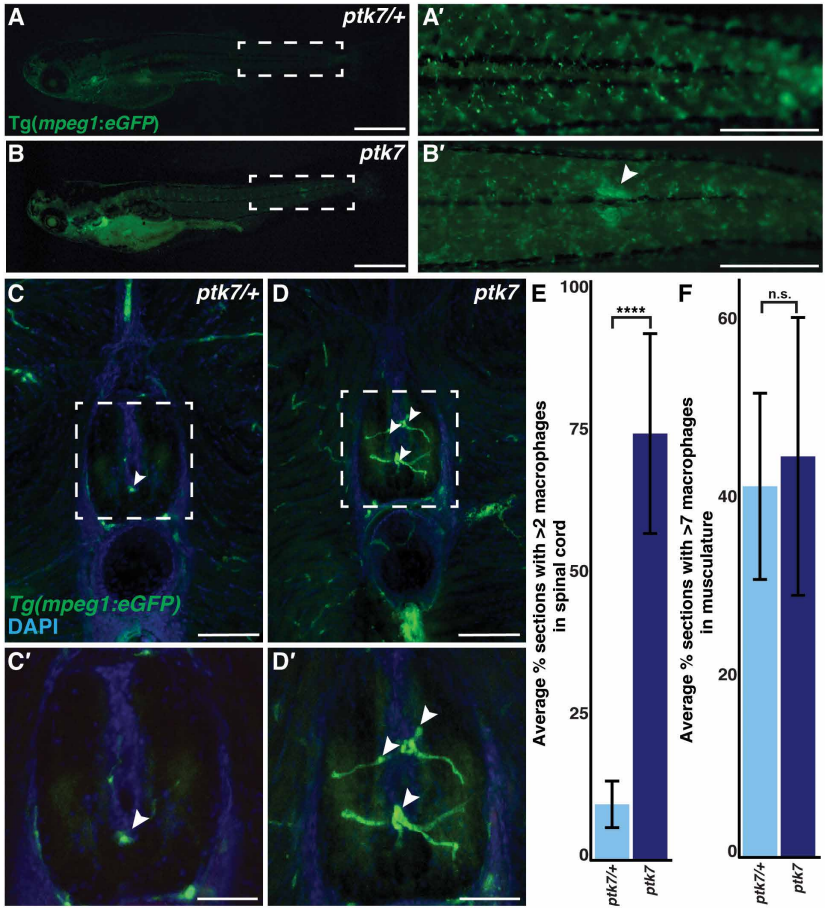

Fig. 3. Macrophages accumulate within the spinal cord of *ptk7* mutants. (**A** and **B**) Whole-mount fluorescent images of Tg(*mpeg1:eGFP*) macrophage reporter expression in *ptk7*/+ [*n* = 10 of 10 (A)] and *ptk7* mutant fish [*n* = 14 of 15 (B)]. Dashed boxes indicate magnified regions (A′ and B′). (**C** and **D**) Transverse sections through 18-dpf *ptk7*/+ and *ptk7* mutant fish demonstrating *GFP*$^+$ macrophage accumulation within the spinal cord of *ptk7* mutants. Dashed boxes indicate magnified regions of spinal cord (C′ and D′). (**E**) Plot demonstrating significant increase in the percentage of sections with greater than two macrophages within the spinal cord for *ptk7* mutant (*n* = 260 sections from 10 fish) versus *ptk7*/+ controls (*n* = 151 sections from 5 fish) (****$P < 0.0001$). (**F**) No significant difference ($P = 0.4273$) between the percentage of sections with greater than seven macrophages within the muscle area for *ptk7*/+ (*n* = 146 sections from 5 fish) and *ptk7* (*n* = 248 sections from 10 fish) mutants. Note that two and seven represent the average number of macrophage observed in control spinal cord and muscle tissues, respectively (fig. S5). Scale bars, 1 mm (A and B), 0.5 mm (A′ and B′), 100 μm (C and D), and 50 μm (C′ and D′).

within the spinal cord of *ptk7* mutant fish (Fig. 3, C to F, and fig. S5). These results, in conjunction with RNA-seq data, suggest that *ptk7* mutants experience a neuroinflammatory response at the onset of spinal curve formation.

Focal neuroinflammatory signals are sufficient to induce IS-like spinal curvature

If neuroinflammation drives scoliosis in *ptk7* mutant fish, then induction of immune responses within the spinal cord of wild-type animals should be sufficient to cause spinal curvature. To test this, we generated CNS expression clones of (i) the proinflammatory cytokine interferon-γ 1-2 (*ifng1-2*) (*21*) and (ii) mCherry-tagged immunoresponsive gene 1-like (*irg1l*), which regulates macrophage and neutrophil recruitment to wounded epithelia (*22*) and is strongly upregulated in scoliotic *ptk7* mutants (Fig. 2, D and E). We constructed Tol2-based transposable elements composed of a ubiquitous β*actin2* promoter driving expression of a floxed eGFP reporter element (*loxP-eGFP-loxP* or *LGSL*) followed by *ifng1-2* or *mCherry-irg1l* cassettes. When these transposons are injected into one-cell–staged embryos, widespread and mosaic eGFP expression can be detected (Fig. 4, A, C, and D, and fig. S6). However, within the spinal cord of Tg(*foxj1a::iCre*) embryos, lineage-specific Cre recombinase activity results in recombination of reporter elements, focal expression of proinflammatory molecules, and local recruitment of *eGFP*$^+$ macrophage (Fig. 4C and fig. S6, B and C‴).

To determine whether CNS-specific expression of proinflammatory cues can induce scoliosis, injected embryos were raised and screened for reporter expression and spinal curve formation (Fig. 4).

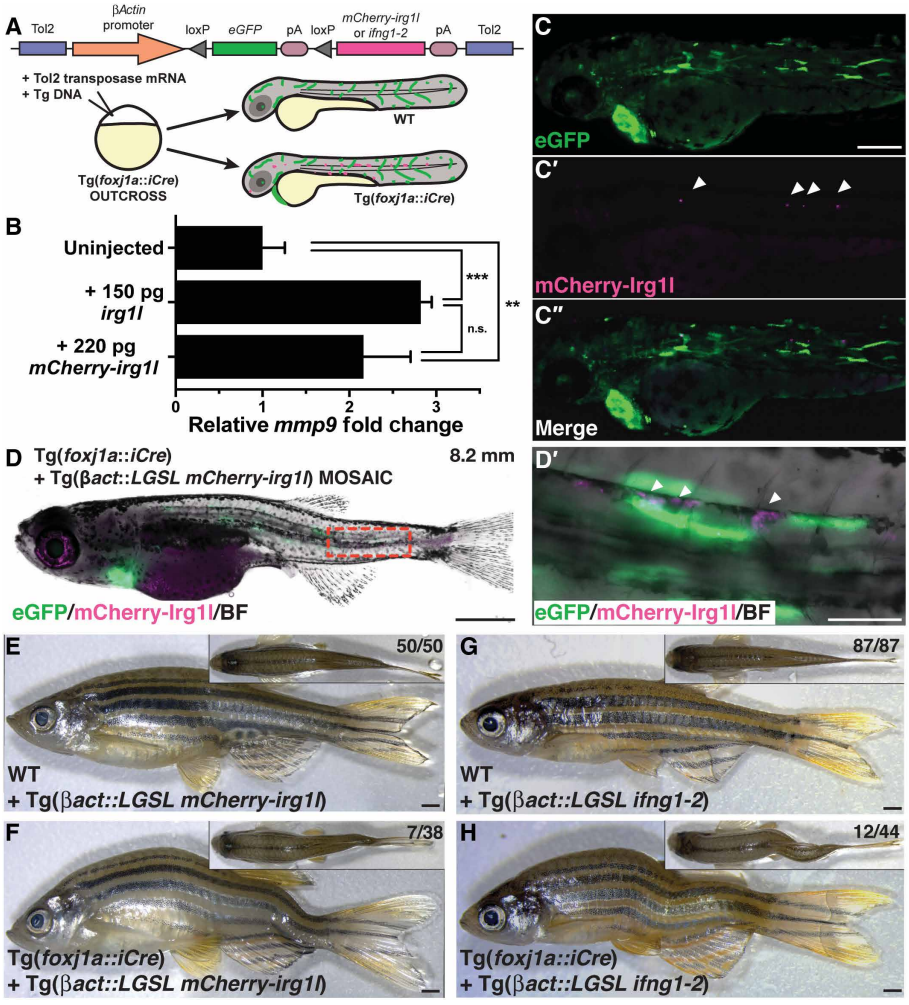

Fig. 4. Proinflammatory cues within the CNS are sufficient to induce scoliotic curves. (**A**) Schematic of Tg(β*act::LGSL mCherry-irg1l*) or Tg(β*act::LGSL ifng1-2*) and the mosaic transposon approach used to generate clones of *irg1l*-expressing cells within *foxj1a*$^+$ lineages. (**B**) qRT-PCR demonstrating functionality of *mCherry-irg1l* fusion construct. Significant up-regulation of the Irg1l target gene *mmp9* is observed upon overexpression of equimolar amounts of both *irg1l* ($P < 0.0004$, two-tailed *t* test) and *mCherry-irg1l* ($P < 0.0284$, two-tailed *t* test) mRNA. Error bars represent the SE for the expression level fold change. ** $P < 0.01$, *** $P < 0.001$. (**C** and **C″**) Representative Tg(*foxj1a::iCre*) embryo at 72 hours post-fertilization (hpf) injected at the one-cell stage using mosaic labeling strategy. Arrowheads indicate clonal populations of mCherry-Irg1l–expressing cells within the *foxj1a*$^+$ lineage (C′). (**D** and **D′**) Juvenile experimental fish develop spinal curvatures with mCherry-Irgl1$^+$ cells visible at the site of curvature. Red rectangle indicates the area shown in higher magnification (D′). Arrowheads indicate clonal populations of mCherry-Irg1l–expressing cells within the *foxj1a*$^+$ lineage. (**E** and **F**) Wild-type (WT) sibling controls injected with Tg(β*act::LGSL mCherry-irg1l*) develop normally (E), whereas Tg(*foxj1a::iCre*) animals develop scoliosis (F). (**G** and **H**) Wild-type sibling controls injected with Tg(β*act::LGSL ifng1-2*) develop normally (G), whereas Tg(*foxj1a::iCre*) fish develop scoliosis (H). Scale bars, 200 μm (C, C″, and D′) and 1 mm (D and E to H). (D to H) Photo Credit: C. W. Boswell, The Hospital for Sick Children.

Injected Cre-negative animals demonstrated mosaic expression of eGFP across all tissues and failed to develop scoliosis (Fig. 4, E and G; $n = 137$). In contrast, Tg(*foxj1a::iCre*) animals injected with Tg(β*act*::*LGSL mCherry-irg1l*) developed spinal curvatures at 3 weeks post fertilization (Fig. 4F; $n = 7$ of 38), suggesting that recombination of the *eGFP* cassette and resulting *mCherry-irg1l* expression in *foxj1a*$^+$ lineages is sufficient to induce spine curvature. Notably, small clones of mCherry-Irg1l$^+$ cells could be identified in the CNS at the apex of developing axial curvatures (Fig. 4D). Similarly, Tg(*foxj1a::iCre*) animals injected with Tg(β*act*::*LGSL ifng1-2*) also developed scoliosis (Fig. 4H; $n = 12$ of 44). The association between proinflammatory signals and spinal curvature is specific to the CNS, as mosaic endothelial-specific expression of *mCherry-irg1l* (fig. S6, D to G; $n = 53$ of 53) or *ifng1-2* failed to cause scoliosis. Together, our data suggest that focal, neuroinflammatory signals are sufficient to drive idiopathic-like spinal curvatures.

Simple immunomodulating therapies suppress scoliosis onset and curve severity

To determine whether suppression of inflammatory responses can block scoliosis in our IS model, *ptk7* mutant zebrafish were treated with the nonsteroidal anti-inflammatory drug (NSAID) acetylsalicylic acid (aspirin). Aspirin was administered to juvenile fish at 10 days of age (~4 mm standard length), before the onset of spinal curvatures, through simple dispensation into tank water at a final concentration of 100 mg/liter. Control and experimental cohorts were reared in tanks isolated from the central recirculatory system, water was changed daily, and aspirin was administered continuously for 30 days. Administration of aspirin to control *ptk7*/+ fish had no adverse effects ($n = 250$). Strikingly, aspirin treatment resulted in a significant reduction in the overall incidence of scoliosis from 92% ($n = 80$ of 87) in untreated controls to only 64% ($n = 67$ of 104) in the experimental cohort (30% reduction in incidence; Fig. 5A). Notably, after removal from aspirin treatment at 40 dpf, 95% of the nonscoliotic *ptk7* mutant fish subsequently developed spinal curvatures. If *ptk7* mutant fish developed spinal curvatures during aspirin treatment, then the average age of scoliosis onset increased from 23 to 35 days (52% change; Fig. 5B). However, quantification of curve magnitude by Cobb angle measurements (fig. S7) (*1*), at 30 days after curve onset, showed a trend but no significant reduction in spinal curve severity between aspirin-treated and control cohorts (Fig. 5C). Together, these data suggest that aspirin treatment can positively affect both the incidence and age of scoliosis onset, but not the severity of spinal curve progression.

Differential gene expression analysis of *ptk7* mutant siblings with severe versus mild scoliosis identified up-regulation of *nos2a* as the largest and most significant variance associated with severe spinal curvature (data file S1). Given our previous observations of up-regulated *nox1* and *irg1l* expression in severe *ptk7* mutants (Fig. 2) and their established gene functions in reactive oxygen species generation, we hypothesized that oxidative stress may influence spinal curve progression. To test this, we treated *ptk7* mutants with *N*-acetylcysteine (NAC), a widely available, over-the-counter supplement with both antioxidant and anti-inflammatory properties (*23*, *24*). As described for aspirin treatment, NAC was administered to juvenile fish beginning at 7 days of age (~3 mm standard length, before scoliosis onset) through 40 days of age, via simple dispensation into tank water at a final concentration of 200 mg/liter. Notably, by 40 dpf, only 17% ($n = 8$ of 47) of NAC-treated *ptk7* mutants had developed spinal curvatures compared to 81% ($n = 77$ of 95) of the control population (79% reduction in incidence; Fig. 6A). Moreover, removal of NAC from the experimental cohort resulted in rapid onset of scoliosis in 49% of animals (Fig. 6A; $n = 19$ of 39). These data indicate a significant and specific role for NAC treatment in suppressing spinal curve formation.

The low penetrance of scoliosis in the NAC-treated cohort precluded meaningful statistical analysis of spinal curve severity. We therefore devised a treatment regimen whereby fish were not administered NAC until after spinal curve onset (Fig. 6B). *ptk7* mutants were censused daily and, upon onset of scoliosis, removed from the population and split into experimental and control groups. Experimental cohorts were administered NAC (200 mg/liter), as described above. All fish were then collected at 20 days after curve onset to assess curve severity (fig. S7). Treatment with NAC after scoliosis onset significantly reduced the severity of spinal curve progression (Fig. 6C).

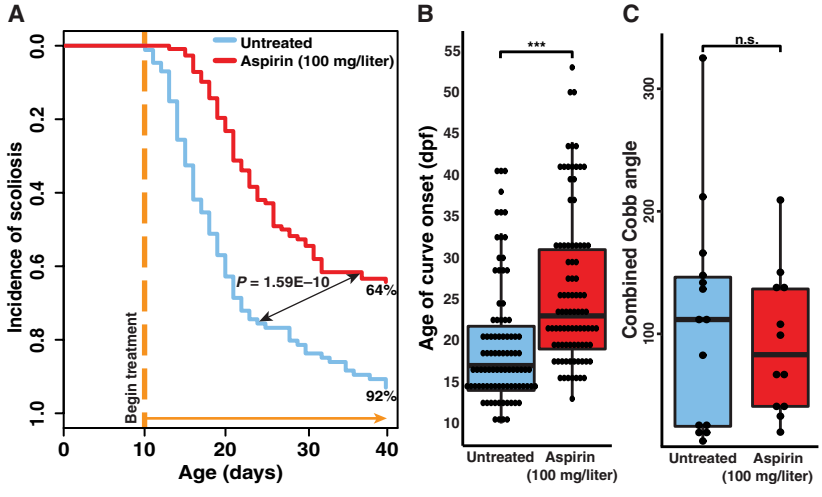

Fig. 5. Aspirin treatment significantly affects spinal curve formation. (**A**) Kaplan-Meier estimator analysis demonstrating significant differences in the incidence and onset of scoliosis in control ($n = 87$) versus aspirin-treated ($n = 111$) *ptk7* mutant fish ($N = 5$). (**B**) Box and whisker plot demonstrating a significant difference in the age of scoliosis onset between control ($n = 90$) and aspirin-treated ($n = 88$) *ptk7* mutants ($P = 1.8 \times 10^{-7}$, two-tailed *t* test). *** $P < 0.001$. (**C**) Scoliotic fish were fixed at 30 days after phenotype onset to assess curve severity. Quantification of combined Cobb angles in untreated ($n = 14$) versus aspirin-treated ($n = 12$) *ptk7* scoliotic fish revealed no significant difference in curve severity ($P = 0.1779$, two-tailed *t* test).

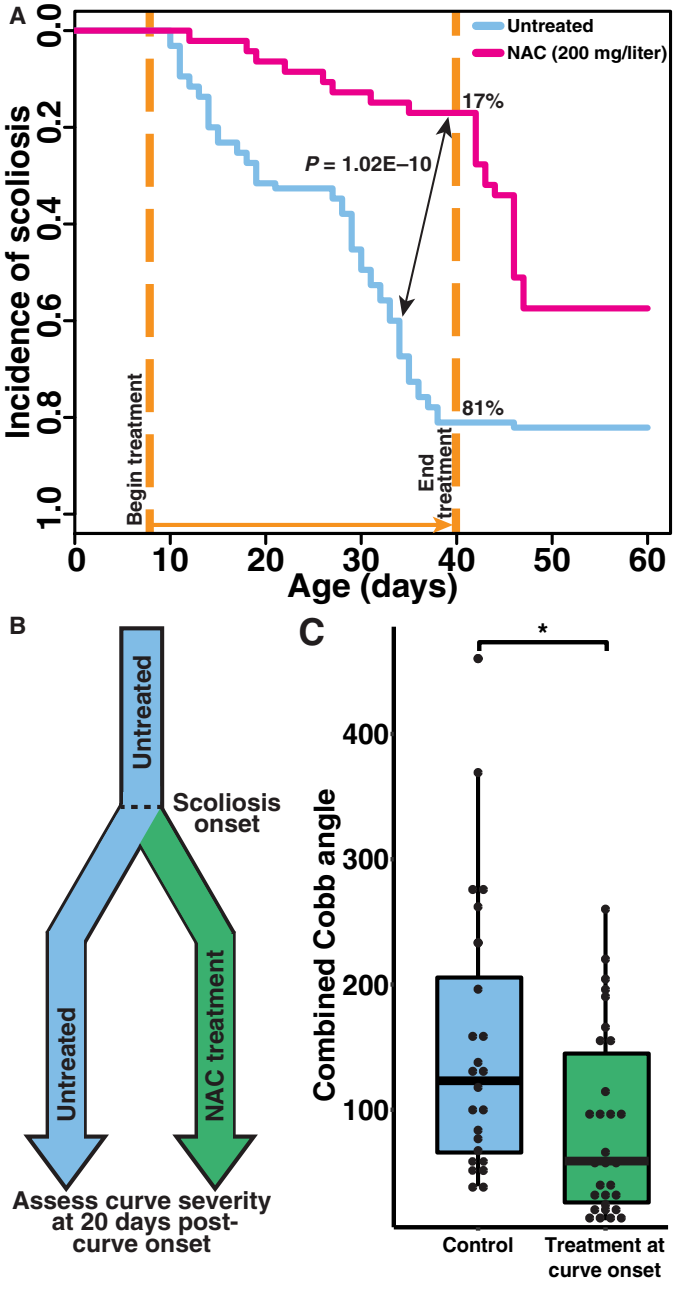

Fig. 6. NAC treatment significantly prevents spinal curve formation and progression. (**A**) Kaplan-Meier estimator analysis demonstrating significant differences in the incidence and onset of scoliosis in control ($n = 95$) versus NAC-treated ($n = 47$) *ptk7* mutant fish. (**B**) Schematic representing the treatment at curve onset administration plan. Fish in the control are untreated and collected at 20 days after curve onset to assess curve magnitude. Fish in the treatment at onset cohort are administered NAC (200 mg/liter) when spinal curvatures are observed and then collected at 20 days after curve onset and curve severity are assessed. (**C**) Quantification of combined Cobb angles in untreated *ptk7* fish ($n = 24$) and *ptk7* fish treated with NAC at curve onset ($n = 31$) displayed a significant decrease in curve severity with NAC treatment ($P = 0.0119$, two-tailed *t* test). *$P < 0.05$.

DISCUSSION

Together, our results implicate neuroinflammatory signals as the pathobiological mechanism driving idiopathic-like spinal curve formation in zebrafish models of IS. In *ptk7* mutant animals, we postulate that neuroinflammation is caused by focal neurodegeneration or demyelination events, which occur in the spinal cord downstream of observed CSF flow and/or homeostasis defects. How proinflammatory signals within the CNS ultimately influence spine development remains to be determined. Irregularities in the distribution of cytokines/signals within the CSF, or perhaps asymmetric hydrodynamic forces operating within the central canal of the spinal cord, must be relayed to overlying musculature and axial skeleton to induce curvatures. Notably, an evolutionarily conserved population of neurons called "CSF-contacting neurons" (CSF-cNs) line the central canal of the spinal cord, project a sensory cilia into the CSF, and can detect changes in pH as well as physical curvature of the body axis (*25*–*29*). Although the function of CSF-cNs is not well understood, they have been demonstrated to modulate spinal circuits that underlie locomotion and posture, and zebrafish *pkd2l1* mutations, which compromise mechanosensory functions of CSF-cNs, have recently been associated with exaggerated spine curvatures (*26*, *30*). Because CSF-cNs are uniquely situated to both detect CSF abnormalities within the central canal and influence overlying muscular contraction, we have hypothesized that abnormal CSF-cN activity (i.e., in response to physical changes to CSF flow or chemical composition, downstream of proinflammatory signals) may contribute to spinal curve progression (*8*).

Although a definitive link between neuroinflammation and human IS requires further study, inflammatory origins of scoliosis are not inconsistent with human clinical and genetic studies. Hyper-IgE (immunoglobulin E) syndrome, characterized by frequent bacterial infection and inflammation, has been associated with developmental scoliosis (*31*). Similarly, more than 50% of patients characterized by recurring nontuberculosis mycobacterial infection present with idiopathic-like spinal curvatures (*32*). To date, the biological consequences of most IS-associated variants identified in genetic and genome-wide association studies remain uncertain (*1*). For example, IS-associated variants linked to *GPR126* have been functionally interrogated largely in the context of musculoskeletal origins of scoliosis (*4*, *33*). However, because myelination requires GPR126 (*34*), regional demyelinating events downstream of *GPR126* dysfunction could activate microglial inflammatory signals that initiate IS-like spinal curvature. Novel neuroinflammatory origins of IS identified in this study thus warrant a reexamination and interpretation of human IS clinical and genetic data.

Strikingly, we have demonstrated that treatment with common NSAIDs can have a significant and positive impact on the incidence and severity of scoliosis in our *ptk7* mutant models. Notably, prophylactic treatment with NAC reduced the incidence of scoliosis in experimental cohorts by 79%. Furthermore, administration of NAC after scoliosis onset significantly reduced the severity of spinal curve progression. NAC is considered a well-tolerated and safe medication, with emerging clinical use for treating neurological and neurodevelopmental disorders in both children and adults [reviewed in (*23*, *35*)]. The therapeutic potential of NAC in treating IS remains to be determined. However, given that simple immunomodulating therapies prove effective in managing zebrafish idiopathic-like spinal deformities, conservation of the mechanism could have profound impacts on the future prevention and treatment of human scoliosis.

MATERIALS AND METHODS

Animal care

Zebrafish husbandry and experimental protocols were approved by the Hospital for Sick Children's Animal Care Committee, and all

protocols were performed in accordance with Canadian Council on Animal Care guidelines. *ptk7*^{hsc9} (*9*), Tg(*foxj1a*::*ptk7*)^{hsc12} (*12*), Tg(*ubi:Switch*)^{cz1701Tg} (*16*), Tg(*hsp*:*Cre*)^{a134} (*17*), Tg(*mpeg1*:*eGFP*)^{gl22} (*20*), and Tg(*kdrl*:*Cre*)^{s898} (*36*) mutant and transgenic fish used in this study have been previously described.

Molecular cloning

A full-length open reading frame (ORF) of *irg1l* was amplified from complementary DNA template prepared from 3-dpf zebrafish embryo RNA using SuperScript IV following the manufacturer's instructions using primers GGGGACAGCTTTCTTGTACAAAGTGGGGGCCACCATGCTTTCAGCGGTACAGAGATC (forward) and GGGGACAACTTTGTATAATAAAGTTGCTTATTGCAGTTGGGCAAGCAG (reverse). An *ifng1-2* ORF was amplified from pTol2-hsp70:*ifng1-2-V5* (a gift from S. Sawamiphak and D. Stainier) using the following primers: GGGGACAGCTTTCTTGTACAAAGTGGTCGCCACCATGATTGCGCAACACATG (forward) and GGGGACAACTTTGTATAATAAAGTTGCTCAACCTCTATTTAGACTTTTGCT (reverse).

Both amplicons were gel extracted and recombined into pDONR P2rP3 via Gateway technology (Invitrogen) to generate p3E-*irg1l* and p3E-*ifng1-2*. The p3E-*irg1l* plasmid was further modified by introducing an N-terminal mCherry and a (GGGGS)×3 linker fusion by megaprimer PCR to generate p3E-*mCherry-irg1l*. To generate pME-*loxP-eGFP-pA-loxP* (referred to as *LGSL*), the cassette was amplified from pENTR5′_ubi:loxP-EGFP-loxP (Addgene plasmid no. 27322) (*16*) and recombined into pDONR221. pME-*loxP-mCerulean-pA-loxP* was generated by replacing the eGFP ORF in pME-*loxP-eGFP-pA-loxP* with mCerulean via Not I/Nco I digestion and ligation. Plasmids were sequence verified before downstream assembly.

Quantitative reverse transcription polymerase chain reaction

qRT-PCR for RNA-seq verification was performed using 10 ng of total RNA in a one-step qRT-PCR [Luna Universal One-Step RT-qPCR Kit, New England Biolabs (NEB)] and performed on a Roche LightCycler 96 system. Primers were designed for verifying some of the up-regulated and immune-related genes (see table S1 for primers used). All graphs are representative of two independent experiments with three technical replicates.

Functional testing of mCherry-irg1l fusion protein was performed by RNA overexpression, followed by qRT-PCR assays of *mmp9* target gene induction (*22*). Briefly, untagged *irg1l* and *mCherry-irg1l* were subcloned into pCS2^{+} vectors and used as templates for in vitro transcription. Equimolar amounts of each RNA were injected into one-cell–staged embryos, and total RNA was extracted from 50 embryos at 28 hpf using TRIzol reagent (catalog no. 15596026, Invitrogen) following the manufacturer's recommendations. Total RNA (100 ng) was used in a one-step qRT-PCR (Luna Universal One-Step RT-qPCR Kit, NEB) and performed on a Roche LightCycler 96 system. All analyses were carried out in triplicate. Results are representative of two independent experiments with three technical replicates each. See table S1 for primer sequences.

Transgenesis

The Cre-excisable destination vector pDEST Tol2LGSR was generated from pDEST Tol2pA2. A fragment encoding for the zebrafish γ-crystallin promoter, *eGFP*, loxP site, and overlapping sequence was purchased and synthesized from Blue Heron Gene Synthesis, digested with Bgl II and Nco I (NEB), and ligated into the corresponding sites in pDEST Tol2pA2 to generate an intermediate vector. A second fragment encoding for a loxP site, *mCherry*, and overlapping sequence was purchased and synthesized similarly, digested with Nsi I and Sal I (NEB), and ligated into the intermediate vector to generate the final Gateway-compatible pDEST Tol2LGSR. This vector permits Cre-dependent removal of transgenes with a visual readout of lens color change. Upon the introduction of Cre recombinase, transgene cassettes that reside between the vector loxP sites are excised with the GFP, resulting in mCherry being driven by the γ-crystallin promoter.

Final transgenes were assembled using standard Tol2 kit Gateway-compatible vectors via LR reactions (*37*). To generate Tg(*foxj1a*::*iCre*) zebrafish, p5E-*foxj1aP* (*12*), pME-iCre (a gift from K. Kwan), and p3E-polyA were recombined into pDEST Tol2 CG2 transgenesis vector. To generate Tg(floxed-*foxj1a*::*ptk7*) zebrafish, p5E-*foxj1aP* (*12*), pME-*ptk7* (*9*), and p3E-polyA were recombined into pDEST Tol2LGSR transgenesis vector. Embryos were injected at the one-cell stage with 25 pg of assembled transgene and 25 pg of Tol2 mRNA. Embryos were sorted at 48 hpf for reporter expression (GFP^{+} hearts or eyes) and were subsequently grown to adulthood. Individuals were bred to TU wild-type zebrafish to generate stable F1 lines. Subsequent F1 lines harboring Tg(floxed-*foxj1a*::*ptk7*) were bred and maintained in *ptk7*^{hsc9} mutants. Two independent Tg(*foxj1a*::*iCre*) lines that had equivalent expression were generated.

Imaging

Imaging of double transgenic Tg(*ubi*:*Switch*);Tg(*foxj1a*::*iCre*) animals was performed on an Axio Zoom.V16 and an LSM 710 confocal microscope (Zeiss). Z-stacks were collected and processed in Zen (Zeiss).

Global and local heat shocks

Global heat shocking was performed by rapidly immersing 2.5-dpf embryos into 38°C egg water for 30 min, followed by gradual recovery to 28.5°C. Embryos were screened for successful heat shocking by recombination of the eGFP to mCherry lens reporter and grown to adulthood. Local heat shocking was performed by using a modified soldering iron (SP12 Mini Soldering Iron, Weller) connected to a DC regulated power supply (Digital Triple Output DC Power Supply, Extech). Soldering iron tips were calibrated for temperature using a soldering tip thermometer (Digital Solder Tip Celsius Thermometer, Hakko FG100), and voltage output was set to 22.5 V corresponding to 44°C (as warmer temperatures were required for heat shock induction because of tip cooling after immersion into egg water). Before heat shock, embryos were aligned in an agarose plate with wells containing egg water, with tricaine anaesthetic either head-up for head heat shocks or tail-up for trunk heat shocks. Local heat shocking was performed by resting the soldering iron tip on the embryos for 3 min per individual embryo, followed by removal from the agarose plate and recovery at 28.5°C. Embryos were screened for successful heat shock induction by recombination of the eGFP to mCherry *ubi*:*Switch* reporter and grown to adulthood. See fig. S2 for experimental setup.

Transposon-mediated clonal expression

Cre-dependent transposons used in mosaic clonal expression were assembled using standard Tol2 kit Gateway-compatible vectors via LR reactions. To generate Tg(β*actin2*::*LGSL mCherry-irg1l*), p5E-β*actin2* (*37*), pME-*loxP-eGFP-pA-loxP*, and p3E-*mCherry-irg1L* were recombined into pDEST Tol2 pA2 transgenesis vector. To generate

Tg(β*actin2*::*LGSL ifng1-2*), p5E-β*actin2*, pME-*loxP-eGFP-pA-loxP*, and p3E-*ifng1-2* were recombined into pDEST Tol2 pA2 destination vector. Embryos produced from a Tg(*foxj1a*::*iCre*) outcross were injected at the one-cell stage with 12 pg of either Tg(β*actin2*::*LGSL mCherry-irg1l*) or Tg(β*actin2*::*LGSL ifng1-2*) and 12 pg of Tol2 mRNA. Embryos were sorted at 48 hpf for Cre reporter expression (GFP^+ hearts and GFP^- hearts for Cre^+ and Cre^- cohorts, respectively). In experiments using Tg(β*actin2*::*LGSL mCherry-irg1l*), embryos were further screened at 72 hpf for $mCherry^+$ cells within *foxj1a*$^+$ lineages representing clones expressing mCherry-Irg1l fusion protein. Embryos devoid of $mCherry^+$ cells were excluded from the analysis. Cohorts were grown to adult stages and assessed for scoliotic phenotypes. Embryonic and juvenile imaging was performed on an Axio Zoom.V16 (Zeiss).

For imaging macrophage recruitment upon proinflammatory expression, a Cre-dependent transposon was assembled using p5E-β*actin2*, pME-*loxP-mCerulean-pA-loxP*, and p3E-*mCherry-irg1l* into pDEST Tol2 pA2 transgenesis vector. Embryos produced from a intercross between Tg(*mpeg1*:*eGFP)* and Tg(*foxj1a*::*iCre*) animals were injected at the one-cell stage with 12 pg of assembled transgene and 12 pg of Tol2 mRNA, sorted at 48 hpf for Cre reporter expression, and imaged for eGFP, mCerulean, and mCherry on a A1r confocal microscope (Nikon).

RNA sequencing

Experimental animals were euthanized with tricaine (500 mg/liter; MS-222/MESAB), followed by submersion of anesthetized fish in ice water for several minutes. Once morbidity was assured, the head was removed just behind the gill using a scalpel, and a fin clip was collected for genotyping. The trunk and tail specimens were preserved in RNA*later* RNA Stabilization Reagent (RNeasy Mini Kit, Qiagen) until RNA extraction could be performed (once genotyping was complete). Total RNA extraction was performed using a Qiagen RNeasy kit following the manufacturer's instructions (Qiagen). RNA sample quality was assessed using an Agilent Bioanalyzer. Library preparation and subsequent sequencing was performed by The Centre for Applied Genomics at The Hospital for Sick Children (SickKids) using the NEBNext stranded RNA. Libraries were sequenced on an Illumina HiSeq2500 sequencer according to the manufacturer's instructions, with paired end reads and read lengths of 100 bp. Read quality was assessed using FastQC, and adaptors were trimmed from reads using Cutadapt. Reads were then reassessed for quality using FastQC. Reads were aligned to the zebrafish genome (GRCz9) using RNAStar and converted to bam files using Samtools.

For *ptk7*/+ versus *ptk7* mutant with severe scoliosis RNA-seq experiments, fish were collected at ~1 cm in standard length. Three severe curve *ptk7* mutants and three straight spine *ptk7*/+ fish, which were of similar lengths, were selected and processed for RNA-seq differential gene expression analysis (see below). RNA-seq yielded approximately 30 million reads per sample.

Fish for *ptk7* + Tg(*foxj1a*::*ptk7*) versus *ptk7* mutants at scoliosis onset RNA-seq experiments were collected at ~0.7 cm in length. 6 *ptk7* mutants with nascent spinal curvatures and 6 *ptk7* + Tg(*foxj1a*::*ptk7*) fish with straight spines were selected and processed for RNA-seq differential gene expression analysis. RNA-seq yielded approximately 60 to 70 million reads per sample.

For *ptk7* + Tg(*foxj1a*::*ptk7*) versus *ptk7* mutants with mild or severe scoliosis, fish were collected at ~0.8 cm in length. Four *ptk7* mutants with severe curve, four *ptk7* mutants with mild curves, and three *ptk7* + Tg(*foxj1a*::*ptk7*) were selected and processed for RNA-seq differential gene expression analysis. RNA-seq yielded approximately 60 to 70 million reads per sample.

RNA-seq differential gene expression analysis

Aligned reads were quantified using SeqMonk. Differential gene expression analysis was performed with the Bioconductor package DESeq2. GO term enrichment analysis was acquired using the PANTHER classification system and PANTHER Tools gene list analysis. The heatmap was created using R. Lists of genes annotated with "GO:0006953 Acute-phase response," "GO:0006956 Complement activation," and "GO:0006954 Inflammatory response" were downloaded from the Gene Ontology Consortium (*38*), and genes within these lists, which were significantly ($P < 0.05$) up-regulated at onset of scoliosis, at mild curvature, or at severe curvature, were chosen to create the heatmap. Volcano plots were created using R, and lists of genes for associated GO terms were downloaded from the Gene Ontology Consortium.

Drug and chemical treatments

Fish for chemical/drug treatments were housed off-system in 1 liter of system water in 6-liter tanks with up to 40 fish per tank, and water was changed once per day. Acetylsalicylic acid (100 mg; CAS 50-78-2, Sigma-Aldrich) was administered once per day to experimental fish during water changes. NAC (CAS 616-91-1, Sigma-Aldrich) was prepared in a stock solution of 10 g/liter in system water and brought up to a pH of 7 with NaOH and then stored at 4°C. NAC was administered once per day at a final concentration of 200 mg/liter with water changes. Fish were fed according to the regular feeding schedule throughout the experiment. During water changes, fish were monitored for onset of scoliosis, and overall length was measured. For analysis of curve severity, fish were separated on the basis of age of curve onset and, at 20 or 30 days after curve onset, fixed in 4% paraformaldehyde in 1× phosphate-buffered saline (PBS) for alizarin red staining.

Alizarin red staining and Cobb angle measurements

Alizarin red staining was performed as previously described (*10*). Cobb angles were measured using SCODIAC software. Cobb angle measurements from lateral and dorsal images were summed together to achieve an overall accumulative Cobb angle measurement for each scoliotic fish (fig. S7).

Transverse cross sections and quantification of macrophage localization

Tg(*mpeg1:eGFP*) fish were euthanized and fixed in 4% paraformaldehyde overnight at 4°C. Fish were then stained with alizarin red at room temperature overnight and washed once in 1× PBS. Stained samples were embedded in 4% agarose, and agarose blocks were stored overnight in 1× PBS at 4°C. Sections (150 μm) were obtained using a Leica VT1200S vibrating blade microtome and mounted in Fluoroshield with DAPI (4′,6-diamidino-2-phenylindole; F6057, Sigma-Aldrich). Z-stacks of approximately 50 μm, 1.375-μm step size, were captured for each section using a Nikon A1 confocal microscope with 20× objective. Macrophage numbers were first counted in maximum intensity z-stack projection images of individual sections. Macrophage numbers were verified by reexamining the entire *z*-series to ensure that outstretched processes were properly assigned to individual macrophage cell bodies.

Live fluorescent dye ventricle injections

Fluorescent dye injections were performed using a microinjection apparatus. Two-week-old fish were anesthetized in a dilute solution of tricaine. Anesthetized fish were transferred onto an agarose injection plate in a petri dish filled with anesthetizing agent. Ventricle location was identified using the diamond-shaped pigment pattern on the top of the head, and a glass injection capillary was inserted into that pigment pattern. Approximately 10 nl of nontoxic violet highlighter (*39*) was injected into the ventricle. Injected fish were imaged at 2 hours after injection on an Axio Zoom.V16 (Zeiss).

Statistical analysis

The number of macrophages within the spinal cord, and within the muscle, in *ptk7*/+ and *ptk7* mutant fish was compared using a two-tailed *t* test. $P < 0.05$ was considered to be significant. The *t* test assumes normality, which was analyzed by performing a Q-Q plot for each data set. All data sets were found to be normally distributed. Cobb angle measurements and age of scoliosis onset from *ptk7* mutant fish in untreated and aspirin-treated populations were compared using a two-tailed *t* test, where $P < 0.05$ was considered to be significant. The incidence of scoliosis in control and aspirin-treated populations was compared using the Kaplan-Meier estimator, which is available as part of the R "survival" package. All analyses were performed in R.

For qRT-PCR analysis, C_t values were obtained for target genes and normalized to *EF1a*. Fold change was calculated relative to wild-type expression according to the following equation: $2^{-\Delta\Delta Ct}$. Standard error was calculated as standard deviation of the fold change according to the following equation: $\text{stdev}_{\text{foldchange}} = (\ln 2)(\text{stdev}_{\Delta\Delta Ct})(2^{-\Delta\Delta Ct})$, where $\text{stdev}_{\Delta\Delta Ct} = \sqrt{(\text{stdev of reference})^2 + (\text{stdev of gene of interest})^2}$. Statistical significance was calculated using Student's *t* test.

SUPPLEMENTARY MATERIALS

Supplementary material for this article is available at http://advances.sciencemag.org/cgi/content/full/4/12/eaav1781/DC1

Fig. S1. Cre/lox lineage tracing of *foxj1a*$^+$ cells throughout zebrafish development demarcates all tissues that may be contributing to scoliosis phenotype.

Fig. S2. Floxed rescue transgene can be efficiently excised in vivo to restore scoliosis phenotype in *ptk7* mutants.

Fig. S3. Volcano plots of differential gene expression in *ptk7* mutants with severe curves versus *ptk7*/+ control siblings.

Fig. S4. Volcano plots of differential gene expression in *ptk7* mutants versus *ptk7* + Tg(*foxj1a::ptk7*) siblings at various time points (curve onset, mild curvature, and severe curvature) confirms scoliosis-associated immune response.

Fig. S5. Quantification of macrophage within the spinal cord and muscle of *ptk7*/+ and *ptk7* mutant fish expressing the Tg(*mpeg1:eGFP*) reporter transgene.

Fig. S6. Proinflammatory signals recruit macrophage, but expression within the vasculature is not sufficient to cause scoliosis.

Fig. S7. Measuring Cobb angles to determine spinal curve severity.

Table S1. List of primers used in this study for qRT-PCR analysis.

Data file S1. RNA-seq differential expression analysis results.

Movie S1. *foxj1a*$^+$ cells are broadly present throughout the central and peripheral nervous system.

REFERENCES AND NOTES

1. J. C. Cheng, R. M. Castelein, W. C. Chu, A. J. Danielsson, M. B. Dobbs, T. B. Grivas, C. A. Gurnett, K. D. Luk, A. Moreau, P. O. Newton, I. A. Stokes, S. L. Weinstein, R. G. Burwell, Adolescent idiopathic scoliosis. *Nat. Rev. Dis. Primers* **1**, 15030 (2015).
2. S. A. Patten, P. Margaritte-Jeannin, J.-C. Bernard, E. Alix, A. Labalme, A. Besson, S. L. Girard, K. Fendri, N. Fraisse, B. Biot, C. Poizat, A. Campan-Fournier, K. Abelin-Genevois, V. Cunin, C. Zaouter, M. Liao, R. Lamy, G. Lesca, R. Menassa, C. Marcaillou, M. Letexier, D. Sanlaville, J. Berard, G. A. Rouleau, F. Clerget-Darpoux, P. Drapeau, F. Moldovan, P. Edery, Functional variants of *POC5* identified in patients with idiopathic scoliosis. *J. Clin. Invest.* **125**, 1124–1128 (2015).
3. G. Haller, D. Alvarado, K. Mccall, P. Yang, C. Cruchaga, M. Harms, A. Goate, M. Willing, J. A. Morcuende, E. Baschal, N. H. Miller, C. Wise, M. B. Dobbs, C. A. Gurnett, A polygenic burden of rare variants across extracellular matrix genes among individuals with adolescent idiopathic scoliosis. *Hum. Mol. Genet.* **25**, 202–209 (2016).
4. I. Kou, Y. Takahashi, T. A. Johnson, A. Takahashi, L. Guo, J. Dai, X. Qiu, S. Sharma, A. Takimoto, Y. Ogura, H. Jiang, H. Yan, K. Kono, N. Kawakami, K. Uno, M. Ito, S. Minami, H. Yanagida, H. Taneichi, N. Hosono, T. Tsuji, T. Suzuki, H. Sudo, T. Kotani, I. Yonezawa, D. Londono, D. Gordon, J. A. Herring, K. Watanabe, K. Chiba, N. Kamatani, Q. Jiang, Y. Hiraki, M. Kubo, Y. Toyama, T. Tsunoda, C. A. Wise, Y. Qiu, C. Shukunami, M. Matsumoto, S. Ikegawa, Genetic variants in *GPR126* are associated with adolescent idiopathic scoliosis. *Nat. Genet.* **45**, 676–679 (2013).
5. S. Sharma, D. Londono, W. L. Eckalbar, X. Gao, D. Zhang, K. Mauldin, I. Kou, A. Takahashi, M. Matsumoto, N. Kamiya, K. K. Murphy, R. Cornelia; TSRHC Scoliosis Clinical Group; Japan Scoliosis Clinical Research Group, J. A. Herring, D. Burns, N. Ahituv, S. Ikegawa, D. Gordon, C. A. Wise, A *PAX1* enhancer locus is associated with susceptibility to idiopathic scoliosis in females. *Nat. Commun.* **6**, 6452 (2015).
6. S. Liu, N. Wu, Y. Zuo, Y. Zhou, J. Liu, Z. Liu, W. Chen, G. Liu, Y. Chen, J. Chen, M. Lin, Y. Zhao, Y. Ming, T. Yuan, X. Li, Z. Xia, X. Yang, Y. Ma, J. Zhang, J. Shen, S. Li, Y. Wang, H. Zhao, K. Yu, Y. Zhao, X. Weng, G. Qiu, Z. Wu, Genetic polymorphism of *LBX1* is associated with adolescent idiopathic scoliosis in Northern Chinese Han population. *Spine* **42**, 1125–1129 (2017).
7. Y. Ogura, I. Kou, S. Miura, A. Takahashi, L. Xu, K. Takeda, Y. Takahashi, K. Kono, N. Kawakami, K. Uno, M. Ito, S. Minami, I. Yonezawa, H. Yanagida, H. Taneichi, Z. Zhu, T. Tsuji, T. Suzuki, H. Sudo, T. Kotani, K. Watanabe, N. Hosogane, E. Okada, A. Iida, M. Nakajima, A. Sudo, K. Chiba, Y. Hiraki, Y. Toyama, Y. Qiu, C. Shukunami, Y. Kamatani, M. Kubo, M. Matsumoto, S. Ikegawa, A functional SNP in *BNC2* is associated with adolescent idiopathic scoliosis. *Am. J. Hum. Genet.* **97**, 337–342 (2015).
8. C. W. Boswell, B. Ciruna, Understanding idiopathic scoliosis: A new zebrafish school of thought. *Trends Genet.* **33**, 183–196 (2017).
9. M. Hayes, M. Naito, A. Daulat, S. Angers, B. Ciruna, Ptk7 promotes non-canonical Wnt/PCP-mediated morphogenesis and inhibits Wnt/β-catenin-dependent cell fate decisions during vertebrate development. *Development* **140**, 1807–1818 (2013).
10. M. Hayes, X. Gao, L. X. Yu, N. Paria, R. M. Henkelman, C. A. Wise, B. Ciruna, *ptk7* mutant zebrafish models of congenital and idiopathic scoliosis implicate dysregulated Wnt signalling in disease. *Nat. Commun.* **5**, 4777 (2014).
11. J. B. Wallingford, B. Mitchell, Strange as it may seem: The many links between Wnt-signaling, planar cell polarity, and cilia. *Genes Dev.* **25**, 201–213 (2011).
12. D. T. Grimes, C. W. Boswell, N. F. C. Morante, R. M. Henkelman, R. D. Burdine, B. Ciruna, Zebrafish models of idiopathic scoliosis link cerebrospinal fluid flow defects to spine curvature. *Science* **352**, 1341–1344 (2016).
13. M. P. Kelly, T. J. Guillaume, L. G. Lenke, Spinal deformity associated with Chiari malformation. *Neurosurg. Clin. N. Am.* **26**, 579–585 (2015).
14. R. A. Özerdemoglu, F. Denis, E. E. Transfeldt, Scoliosis associated with syringomyelia: Clinical and radiologic correlation. *Spine* **28**, 1410–1417 (2003).
15. M. Verhoef, H. A. Barf, M. W. M. Post, F. W. A. van Asbeck, R. H. J. M Gooskens, A. J. H. Prevo, Secondary impairments in young adults with spina bifida. *Dev. Med. Child Neurol.* **46**, 420–427 (2004).
16. C. Mosimann, C. K. Kaufman, P. Li, E. K. Pugach, O. J. Tamplin, L. I. Zon, Ubiquitous transgene expression and Cre-based recombination driven by the *ubiquitin* promoter in zebrafish. *Development* **138**, 169–177 (2011).
17. Y. A. Pan, T. Freundlich, T. A. Weissman, D. Schoppik, X. C. Wang, S. Zimmerman, B. Ciruna, J. R. Sanes, J. W. Lichtman, A. F. Schier, Zebrabow: Multispectral cell labeling for cell tracing and lineage analysis in zebrafish. *Development* **140**, 2835–2846 (2013).
18. M. E. Hardy, L. V. Ross, C.-B. Chien, Focal gene misexpression in zebrafish embryos induced by local heat shock using a modified soldering iron. *Dev. Dyn.* **236**, 3071–3076 (2007).
19. T. Brinker, E. Stopa, J. Morrison, P. Klinge, A new look at cerebrospinal fluid circulation. *Fluids Barriers CNS* **11**, 10 (2014).
20. F. Ellett, L. Pase, J. W. Hayman, A. Andrianopoulos, G. J. Lieschke, *mpeg1* promoter transgenes direct macrophage-lineage expression in zebrafish. *Blood* **117**, 49–56 (2011).
21. S. Sawamiphak, Z. Kontarakis, D. Y. R. Stainier, Interferon gamma signaling positively regulates hematopoietic stem cell emergence. *Dev. Cell* **31**, 640–653 (2014).
22. C. J. Hall, R. H. Boyle, X. Sun, S. M. Wicker, J. P. Misa, G. W. Krissansen, C. G. Print, K. E. Crosier, P. S. Crosier, Epidermal cells help coordinate leukocyte migration during inflammation through fatty acid-fuelled matrix metalloproteinase production. *Nat. Commun.* **5**, 3880 (2014).
23. Deepmala, J. Slattery, N. Kumar, L. Delhey, M. Berk, O. Dean, C. Spielholz, R. Frye, Clinical trials of N-acetylcysteine in psychiatry and neurology: A systematic review. *Neurosci. Biobehav. Rev.* **55**, 294–321 (2015).
24. G. F. Rushworth, I. L. Megson, Existing and potential therapeutic uses for N-acetylcysteine: The need for conversion to intracellular glutathione for antioxidant benefits. *Pharmacol. Ther.* **141**, 150–159 (2014).

25. L. Djenoune, H. Khabou, F. Joubert, F. B. Quan, S. N. Figueiredo, L. Bodineau, F. D. Bene, C. Burcklé, H. Tostivint, C. Wyart, Investigation of spinal cerebrospinal fluid-contacting neurons expressing PKD2L1: Evidence for a conserved system from fish to primates. *Front. Neuroanat.* **8**, 26 (2014).
26. U. L. Böhm, A. Prendergast, L. Djenoune, S. N. Figueiredo, J. Gomez, C. Stokes, S. Kaiser, M. Suster, K. Kawakami, M. Charpentier, J.-P. Concordet, J.-P. Rio, F. D. Bene, C. Wyart, CSF-contacting neurons regulate locomotion by relaying mechanical stimuli to spinal circuits. *Nat. Commun.* **7**, 10866 (2016).
27. E. Jalalvand, B. Robertson, H. Tostivint, P. Wallén, S. Grillner, The spinal cord has an intrinsic system for the control of pH. *Curr. Biol.* **26**, 1346–1351 (2016).
28. K. Fidelin, L. Djenoune, C. Stokes, A. Prendergast, J. Gomez, A. Baradel, F. Del Bene, C. Wyart, State-dependent modulation of locomotion by GABAergic spinal sensory neurons. *Curr. Biol.* **25**, 3035–3047 (2015).
29. J. M. Hubbard, U. L. Böhm, A. Prendergast, P.-E. B. Tseng, M. Newman, C. Stokes, C. Wyart, Intraspinal sensory neurons provide powerful inhibition to motor circuits ensuring postural control during locomotion. *Curr. Biol.* **26**, 2841–2853 (2016).
30. J. R. Sternberg, A. E. Prendergast, L. Brosse, Y. Cantaut-Belarif, O. Thouvenin, A. Orts-Del'Immagine, L. Castillo, L. Djenoune, S. Kurisu, J. R. McDearmid, P.-L. Bardet, C. Boccara, H. Okamoto, P. Delmas, C. Wyart, Pkd2l1 is required for mechanoception in cerebrospinal fluid-contacting neurons and maintenance of spine curvature. *Nat. Commun.* **9**, 3804 (2018).
31. A. D. Papanastasiou, S. Mantagos, D. A. Papanastasiou, I. K. Zarkadis, A novel mutation in the signal transducer and activator of transcription 3 (STAT3) gene, in hyper-IgE syndrome. *Mol. Immunol.* **47**, 1629–1634 (2010).
32. M. Kartalija, A. R. Ovrutsky, C. L. Bryan, G. B. Pott, G. Fantuzzi, J. Thomas, M. J. Strand, X. Bai, P. Ramamoorthy, M. S. Rothman, V. Nagabhushanam, M. McDermott, A. R. Levin, A. Frazer-Abel, P. C. Giclas, J. Korner, M. D. Iseman, L. Shapiro, E. D. Chan, Patients with nontuberculous mycobacterial lung disease exhibit unique body and immune phenotypes. *Am. J. Respir. Crit. Care Med.* **187**, 197–205 (2013).
33. C. M. Karner, F. Long, L. Solnica-Krezel, K. R. Monk, R. S. Gray, *Gpr126/Adgrg6* deletion in cartilage models idiopathic scoliosis and pectus excavatum in mice. *Hum. Mol. Genet.* **24**, 4365–4373 (2015).
34. K. R. Monk, K. Oshima, S. Jörs, S. Heller, W. S. Talbot, Gpr126 is essential for peripheral nerve development and myelination in mammals. *Development* **138**, 2673–2680 (2011).
35. R. Bavarsad Shahripour, M. R. Harrigan, A. V. Alexandrov, *N*-acetylcysteine (NAC) in neurological disorders: Mechanisms of action and therapeutic opportunities. *Brain Behav.* **4**, 108–122 (2014).
36. J. Y. Bertrand, N. C. Chi, B. Santoso, S. Teng, D. Y. R. Stainier, D. Traver, Haematopoietic stem cells derive directly from aortic endothelium during development. *Nature* **464**, 108–111 (2010).
37. K. M. Kwan, E. Fujimoto, C. Grabher, B. D. Mangum, M. E. Hardy, D. S. Campbell, J. M. Parant, H. J. Yost, J. P. Kanki, C.-B. Chien, The Tol2kit: A multisite gateway-based construction kit for *Tol2* transposon transgenesis constructs. *Dev. Dyn.* **236**, 3088–3099 (2007).
38. The Gene Ontology Consortium, M. Ashburner, C. A. Ball, J. A. Blake, D. Botstein, H. Butler, J. M. Cherry, A. P. Davis, K. Dolinski, S. S. Dwight, J. T. Eppig, M. A. Harris, D. P. Hill, L. Issel-Tarver, A. Kasarskis, S. Lewis, J. C. Matese, J. E. Richardson, M. Ringwald, G. M. Rubin, G. Sherlock, Gene Ontology: Tool for the unification of biology. *Nat. Genet.* **25**, 25–29 (2000).
39. Y. Takase, R. Tadokoro, Y. Takahashi, Low cost labeling with highlighter ink efficiently visualizes developing blood vessels in avian and mouse embryos. *Dev. Growth Differ.* **55**, 792–801 (2013).

Acknowledgments: We gratefully acknowledge V. Erfani for her technical assistance; S. Knox, A. Salazar, and E. Schimmens for zebrafish care; and S. Sawamiphak for the zebrafish *ifng1-2* clone. **Funding:** This work was supported, in part, by funding from Canadian Institutes of Health Research (CIHR) operating grants to B.C. (MOP-42462 and PJT-148658) and a CIHR Doctoral Research Award to C.W.B. **Author contributions:** J.L.M.V.G., C.W.B., and B.C. designed and conducted the study and wrote the manuscript. J.L.M.V.G. performed and analyzed all RNA-seq–based experiments, drug treatments, and macrophage imaging. C.W.B. performed lineage tracing, conditional gene analysis, and mosaic proinflammatory expression experiments. **Competing interests:** The authors declare that they have no competing interests. **Data and materials availability:** All data needed to evaluate the conclusions in the paper are present in the paper and/or the Supplementary Materials. RNA-seq data are available online from the NIH Sequence Read Archive under the following accession numbers: SRP142542, SRP141415, and SRP144228. Additional data related to this paper may be requested from the authors.

Submitted 21 August 2018
Accepted 12 November 2018
Published 12 December 2018
10.1126/sciadv.aav1781

Citation: J. L. M. Van Gennip, C. W. Boswell, B. Ciruna, Neuroinflammatory signals drive spinal curve formation in zebrafish models of idiopathic scoliosis. *Sci. Adv.* **4**, eaav1781 (2018).

Neuroinflammatory signals drive spinal curve formation in zebrafish models of idiopathic scoliosis

J. L. M. Van Gennip, C. W. Boswell and B. Ciruna

Sci Adv **4** (12), eaav1781.
DOI: 10.1126/sciadv.aav1781